

Visualization of Geologic Stress Perturbations Using Mohr Diagrams

Patricia Crossno, *Member, IEEE*, David H. Rogers, Rebecca M. Brannon, David Coblentz, and Joanne T. Fredrich

Abstract—Huge salt formations, trapping large untapped oil and gas reservoirs, lie in the deepwater region of the Gulf of Mexico. Drilling in this region is high-risk and drilling failures have led to well abandonments, with each costing tens of millions of dollars. Salt tectonics plays a central role in these failures. To explore the geomechanical interactions between salt and the surrounding sand and shale formations, scientists have simulated the stresses in and around salt diapirs in the Gulf of Mexico using nonlinear finite element geomechanical modeling. In this paper, we describe novel techniques developed to visualize the simulated subsurface stress field. We present an adaptation of the Mohr diagram, a traditional paper-and-pencil graphical method long used by the material mechanics community for estimating coordinate transformations for stress tensors, as a new tensor glyph for dynamically exploring tensor variables within three-dimensional finite element models. This interactive glyph can be used as either a probe or a filter through brushing and linking.

Index Terms—Geomechanical modeling, Mohr diagrams, multiple coordinated views, tensor field visualization, tensor glyph.

1 INTRODUCTION

As the United States has sought to increase domestic energy production, oil and gas exploration has expanded into the deepwater portions of the Gulf of Mexico (GoM) where tens of billions of barrels of undiscovered oil are thought to lie near or beneath deeply buried salt formations. Prior to increases in computational power and the development of novel seismic processing techniques in the late 1980s and early 1990s, exploration in this region was impractical. But, with the recent dramatic improvements in subsalt seismic resolution, the deepwater GoM has become a hotbed for the oil and gas industry's exploration and production activities. Nevertheless, exploitation of this frontier still presents technical challenges because of the extreme water and reservoir depths and complex salt tectonics.

Salt formations create natural traps for the accumulation of oil and gas. Highly compacted salt formations have nearly zero porosity, so they form natural barriers to fluid flow and migration. As salt layers are buried and compacted over time, their density remains low compared to that of the surrounding sediments. This makes them buoyant, which creates geological instabilities. During geologic evolution of a sedimentary basin, salt pushes up through surrounding sediments to form domes, pillows, and diapirs, as shown in Fig. 1. Salt cannot sustain deviatoric stresses, so salt continues to move until buoyancy forces are balanced and internal vertical and horizontal stresses are equal (isotropic) [12]. Oil and gas migrating

through surrounding formations becomes trapped against the salt, forming reservoirs.

Drilling failures adjacent to salt diapirs [4], [33], [35] have resulted from the inability to understand and predict the geomechanical interaction between the isotropic stress state of salt diapirs and the deviatoric stress states of the surrounding formations. In the deepwater GoM setting, each well abandoned without reaching target typically costs tens of millions of dollars, so there is a strong motivation to understand these interactions.

Sandia National Laboratories, in partnership with a consortium of oil companies, has initiated a three-dimensional nonlinear finite element geomechanical simulation effort to understand the interactions between massive salt sections and the surrounding exploration targets. This effort is intended to reduce the occurrence of drilling failures, which will have a direct impact on the feasibility of extracting reserves from the deepwater GoM. The goal is to analyze the in situ stress state existing in, and adjacent to, salt bodies before drilling, as well as under producing conditions. These simulations generate three-dimensional fields of real-valued second-order stress tensors, whose visualization is the focus of this paper.

The motivation for our novel visualization approach is to present tensor information in a way that naturally leverages the training, experience, and preexisting mental models of our users. The current application is designed for the material mechanics and geomechanics communities, both of whom are familiar with the Mohr diagram. The Mohr diagram, a paper-and-pencil graphical method for doing coordinate transformations, is taught to undergraduates in introductory courses. We have modernized the Mohr diagram by making it interactive and extended it to succinctly display contextual information. This results in a new visualization capability that offers users a familiar, but highly advanced, tool for data analysis and interpretation.

• P. Crossno, D.H. Rogers, R.M. Brannon, and J.T. Fredrich are with Sandia National Laboratories, PO Box 5800, Albuquerque, NM 87185. E-mail: {pjcross, dhroger, rnbrann, fredrich}@sandia.gov.

• D. Coblentz is with Los Alamos National Laboratories, PO Box 1663, Los Alamos, NM 87545. E-mail: coblentz@lanl.gov.

Manuscript received 16 Nov. 2004; revised 28 Jan. 2005; accepted 29 Mar. 2005; published online 11 July 2005.

For information on obtaining reprints of this article, please send e-mail to: tcvg@computer.org, and reference IEEECS Log Number TVCG-0140-1104.

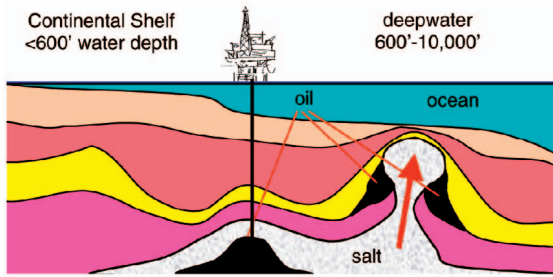


Fig. 1. Salt moves upward to form diapirs, pillows, or vast sheets of salt in response to the instabilities between the salt and the surrounding sediments. Oil accumulates in traps formed below or around the salt diapir.

Most scientific visualizations place tensor information directly into the rendering of the finite element model. Thus, a large number of pixels are needed to view data sets of any size. In contrast, our technique communicates a tremendous amount of information very compactly. Overall contextual data, specific data for a displayed subset, and detailed information about a specific selected element can all be shown simultaneously in the Mohr diagram. Linking this view to a finite element model view allows combined exploration of variables in “FEM space” and tensor values.

The work presented in this paper is an extension of our Visualization 2004 paper [7]. New contributions include a total rewrite of our code into the Visualization Toolkit (VTK) [32], a new user interface written in Trolltech’s Qt [1], and improvements that enable us to handle much larger models. The original application comfortably handled about 10,000 elements, but the new application can handle over a million elements on a single-processor computer. This is critical for the analyst as it enables visualization of the highly complex and extremely large models that are the state of the art in geomechanical modeling [14].

2 TENSOR BASICS

We define a second-order tensor \mathbf{T} to be a 3×3 matrix of values relative to a given “physical” basis:

$$\mathbf{T} = \begin{bmatrix} t_{11} & t_{12} & t_{13} \\ t_{21} & t_{22} & t_{23} \\ t_{31} & t_{32} & t_{33} \end{bmatrix}. \quad (1)$$

Any tensor \mathbf{T} can be decomposed as $\mathbf{T} = \mathbf{S} + \mathbf{A}$, where \mathbf{S} is symmetric ($S_{ij} = S_{ji}$) and \mathbf{A} is skew-symmetric ($A_{ij} = -A_{ji}$). \mathbf{S} represents local force balance, whereas \mathbf{A} balances distributed torques (which are usually zero for the vast majority of engineering applications, making stress typically symmetric). There always exists an alternative basis—the principal basis—in which the off-diagonals of \mathbf{S} are zero and the diagonal components equal the eigenvalues.

After diagonalization of \mathbf{S} , the eigenvalues are λ_1, λ_2 , and λ_3 , ordered so that $\lambda_1 \geq \lambda_2 \geq \lambda_3$; the corresponding orthonormalized eigenvectors are $\mathbf{e}_1, \mathbf{e}_2$, and \mathbf{e}_3 . The eigenvectors are the principal axes of the tensor and are respectively known as the *major*, *medium*, and *minor* axes.

Eigenvalues and eigenvectors have profoundly useful physical meanings that vary depending on the definition of the source tensor \mathbf{S} . If, for example, \mathbf{S} represents a stress,

scaling the eigenvectors by the eigenvalues provides a measure of the forces per unit area in orthonormal directions. There are no shearing stresses on the principal planes; planes of *extremum* shearing stress form equal angles with two principal planes. If \mathbf{S} represents the stretch tensor from a multiplicative decomposition of material deformation, an eigenvalue equals the ratio of deformed length to initial length of the material fiber parallel to the eigenvector. This paper aims at visualizing eigenvalues and eigenvectors in an ensemble sense. We treat \mathbf{S} as a stress tensor, but the techniques apply equally well to any other type of symmetric tensor.

We can determine the types of forces acting on a material element by examining the signs of its tensor’s eigenvalues. If the eigenvalues are all positive, then the forces are tensile, meaning that the element is elongated in tension. If the eigenvalues are all negative, the element is being compressed. If the eigenvalues are of mixed sign, then the element is compressed in some directions and pulled in others. When all of the eigenvalues are equal, $\lambda_1 = \lambda_2 = \lambda_3$, the forces are said to be isotropic and (if the material is also isotropic) the element changes size without changing shape. When the eigenvalues are unequal, the forces are anisotropic.

3 RELATED WORK

Most previous work in tensor visualization falls into one of several categories: glyphs [9], [16], [21], [25], [28], [31], [34], [37], feature-based [19], [27], [36], art-based [24], [26], volume rendered [22], [23], [34], [40], and deformations [3], [39], [40]. Volume rendered and deformation approaches bear little similarity to our work and are not described further.

A number of glyphs have been developed for viewing tensor data. The most common is the ellipsoid, which is drawn using the tensor’s eigenvectors as the principal axes and the eigenvalues to scale the ellipsoid along those axes [25], [31]. Although color-coding to show eigenvalue sign has been tried [38], ellipsoids are generally limited to symmetric, real, positive tensors where all of the eigenvalues are positive. Consequently, they are typically not used to visualize stress fields. Ellipsoids are useful for visualizing diffusion and stretch tensors, though they do have some drawbacks. For data sets where the diffusion rates vary greatly, the smaller ellipsoids virtually disappear [26]. Plus, it is difficult to distinguish between a flattened ellipsoid and a sphere when viewed face on. To overcome this problem, Westin et al. [37] proposed a glyph that is the union of a sphere, a disk, and a rod, the relative size of each encoding a different eigenvalue. Kindmann [21] goes further and creates a continuum of glyphs that use superquadrics to combine the best features of ellipsoids, cuboids, and cylinders.

The Haber glyph [16] is composed of a bar drawn along the principal eigenvector impaling an elliptical disk representing the other eigenvector directions, scaled by the respective eigenvalues. The principal stress hedgehog [20] simply draws the eigenvectors as orthonormal axes scaled by their eigenvalues and colored by eigenvalue sign (red in tension, green in compression). Livingston [28] uses two glyph types, cylindrical tufts and axis tripods, combined with animation and/or depth cueing to visualize

rotation fields. The Reynolds glyph is peanut-shaped and, because the distance from the origin of the glyph surface is determined by the magnitude of the normal stress in that direction, the glyph emphasizes the anisotropy of the tensor [25]. VisCoRe [17] is a framework for visualizing material constitutive relations in geotechnical engineering that uses animated three-dimensional Reynolds glyphs. Glyph-based techniques are best when used on two-dimensional data sets. Glyphs quickly occlude one another in three-dimensional fields for models of reasonable size or complexity.

Clutter is alleviated through the use of probes which interactively move the glyph through the model and change it to reflect the local tensor characteristics. De Leeuw and van Wijk's [9], [31] probe for viewing the velocity gradient tensor in flow fields is one well-known example. It uses a complex icon consisting of an arrow and multiple flexible disks to represent local quantities such as velocity, curvature, and shear. Sigfridsson et al.'s [34] hybrid technique combines texture-based volume rendering with a single ellipsoidal glyph to provide continuous context with detailed tensor information in a region of interest.

Delmarcelle and Hesselink's [10], [25] hyperstreamline glyphs are a type of regional probe. A path is advected through the tensor field along one of the eigenvectors, while, at each step, a tubular surface based on the magnitude and orientation of the other two eigenvectors is drawn. Rather than representing the value of a single tensor, the trumpet-shaped glyph represents a continuum of stresses along the trajectory. Hesselink et al. [19], [27] generated topological skeletons within tensor fields by locating singularities and connecting them with hyperstreamlines integrated along the separatrices. However, even this approach can become cluttered if there are too many hyperstreamlines in the same image. Weinstein et al. [36] developed tensorlines as an alternative feature-following method that better handles propagation through isotropic regions by including nearby orientation information in the path calculation.

Laidlaw et al. [26] present an artistically-based approach that encodes seven attributes of diffusion tensors as different colored layers and types of simulated brush strokes to visualize a two-dimensional slice of a mouse spinal cord. Kirby et al. [24] apply this technique using layered arrows, ellipses, and color to simultaneously visualize multiple attributes in a two-dimensional simulation of flow around a post. In both of these papers, the various brush strokes, or the arrows and ellipses, can be thought of as complex, layered glyphs that provide different information when viewed at different distances.

Although Mohr diagrams are well-known within the materials mechanics and geomechanics communities, they are virtually unknown within the visualization community. The only mention of Mohr diagrams in the visualization literature was in VizCoRe [17], where Mohr's circles are used to represent stress state while doing stress element analysis. However, it appears that their implementation of Mohr's circles is static and does not include interactive features, such as brushing and linking. Advantages of using Mohr diagrams are that they can be applied to tensors with negative eigenvalues [5] and they provide insight into the

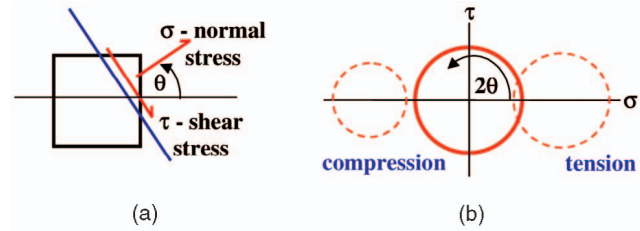


Fig. 2. (a) For a 2D finite element, normal and shear stresses per unit area depend on the orientation of a cutting line. (b) Parametrically plotting normal and shear stresses, σ and τ , as a function of the cutting line's orientation angle, θ , plots a circle (see (2) and (3) below).

local tensor behavior by showing the shear (deviatoric), compressive, and tensile forces.

4 MOHR DIAGRAMS

Otto Mohr developed Mohr diagrams, or Mohr's circles, around 1900 as a graphical method for performing coordinate transformations for stress. Although they were developed to analyze stress, they can be used with any tensor matrix. The method applies to both symmetric and nonsymmetric tensors in two dimensions. However, in three-dimensions, Mohr diagrams are limited to describing just symmetric tensors [5]. We solve this limitation by combining Mohr diagrams with other information (see Section 5).

As an example of how a Mohr's circle captures forces per unit area irrespective of the basis coordinate system, in Fig. 2a, we look at a two-dimensional finite element where normal stress, σ , and shear stress, τ , form orthonormal axes. As we cut through the element with a line oriented by some angle, θ , the measure of normal and shear stress per unit area smoothly changes with the orientation of the line. Mohr proved that parametrically plotting values of σ and τ for every value of θ always draws a circle. The parametric equations for plotting a 2×2 tensor, with component values t_{ij} , are given in (2) and (3) below. Their derivation can be found in the appendix of [5].

$$\sigma(\theta) = \frac{t_{11} + t_{22}}{2} + \frac{t_{11} - t_{22}}{2} \cos 2\theta + \frac{t_{12} + t_{21}}{2} \sin 2\theta, \quad (2)$$

$$\tau(\theta) = - \left(\frac{t_{21} - t_{12}}{2} + \frac{t_{12} + t_{21}}{2} \cos 2\theta + \frac{t_{22} - t_{11}}{2} \sin 2\theta \right). \quad (3)$$

For different tensors, the size and position of the circle will vary depending on the signs and values for σ and τ , as shown by the solid and dashed circles (representing three distinct tensor values) in Fig. 2b.

For three-dimensional symmetric tensors, the Mohr diagram is a triad of circles. However, in keeping with traditional nomenclature, we refer to the entire triad as a Mohr's circle since each triad represents a single tensor. The Mohr diagram is generated by first performing an eigenvalue decomposition of the tensor. For stress tensors, the eigenvectors are normal to planes that are subjected to only normal stress (i.e., zero shear, or deviatoric, stress). If the eigenvalues are not equal, then planes not aligned with the

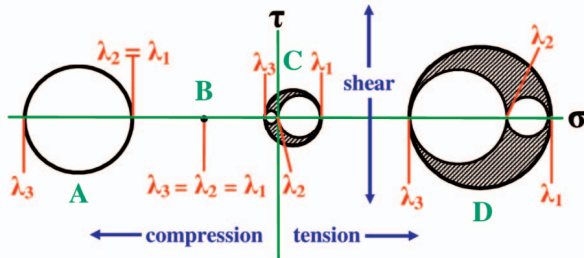


Fig. 3. Four different Mohr's circles representing four different stress tensors with varying degrees of anisotropy, shear, and combinations of compressive and tensile forces. Each tensor's circle triad intersects the σ axis at its eigenvalues. A tensor's maximum shear is seen through the height of its triad's outer circle along the τ axis.

principal directions experience both normal and shearing stresses. Consequently, there exists a state space of shear stress, τ , versus normal stress, σ , characterizing achievable solutions over the infinity of possible orientations of an arbitrary plane cutting through the element. Otto Mohr proved that the set of achievable pairs of τ and σ always fall within the interior of a circle with diameter equal to the difference between largest and smallest eigenvalues; furthermore, attainable stress pairs will always fall outside the circles formed by differences between the extreme and middle eigenvalues. For symmetric tensors, these circles always fall on the normal stress axis, σ . Constructing them is simply a matter of drawing three circles between the eigenvalues. Of course, these circles must fall on the σ axis because principal planes suffer no shear.

In Fig. 3, there are four Mohr's circles (each illustrating different stress tensors) lettered A, B, C, and D. In each, the outer circle is a measure of the degree of anisotropy of the tensor; the larger the circle, the more anisotropic the tensor is (i.e., the greater the peak attainable shear stress). The intersection of the two smaller inner circles shows the value for the medium eigenvector, λ_2 . In A, $\lambda_2 = \lambda_1$, so the larger inner circle overlaps the outer circle and the smaller inner circle goes to a point. Isotropic tensors (B) collapse to a point, showing that there is no shear stress. Both A and B represent degenerate cases used to identify features [27].

The position of the Mohr's circle on the σ axis relative to the origin represents whether the tensor is in compression or tension. Circles that are entirely to the left of the origin are in compression (A and B); those to the right are in tension (D). Circles enclosing the origin represent tensors with a combination of both compressive and tensile forces (C). The shaded regions in C and D show all the achievable solutions for τ and σ within tensors C and D.

5 IMPLEMENTATION OVERVIEW

We have implemented a suite of tools for viewing finite element simulation results, focusing on the domain of nonlinear finite element geomechanical modeling. This work builds upon our earlier visual debugging application [6], [8] and Mohr's circle implementation [7]. Taking advantage of the cross-platform capabilities of VTK and Qt, combined with using CMake [29] as the build system, our new application is delivered on a variety of platforms.

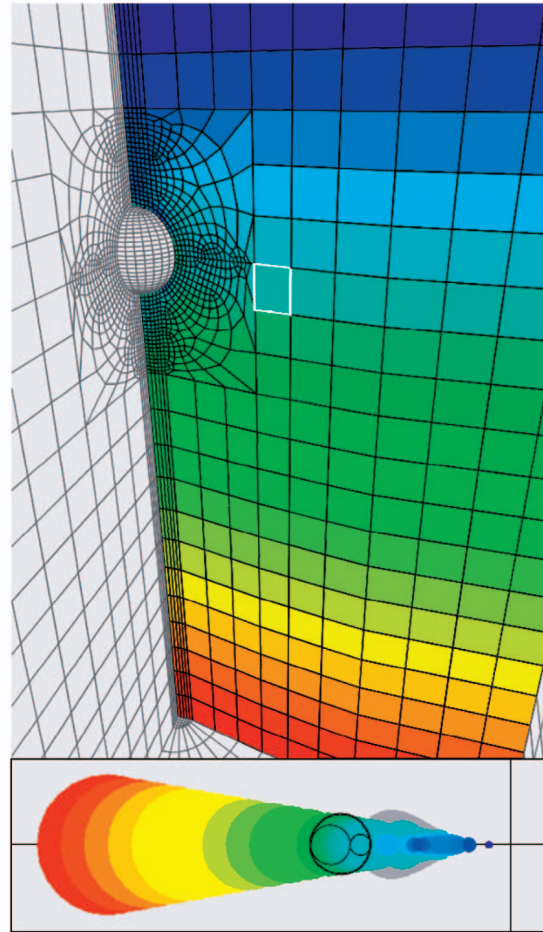


Fig. 4. The upper image shows a colored planar subset of finite elements combined with an outline mesh of the material boundaries for context. The view is from inside of the finite element volume looking towards the boundary between the spherical salt diapir and the surrounding sediments. The elements are color-coded according to the values of the displayed variable (von Mises stress). The lower image shows the Mohr's circles for the subset, color-coded to correspond to the model view. The black Mohr's circle overlaying the colored circles is an interactive probe that updates as the mouse moves over the elements in the upper window. The active element is outlined in white. The Mohr's circle for this element depicts a state of triaxial compression with three disparate eigenvalues. In the colored envelope, the larger cyan circle protruding from the linear ramp of surrounding circles (to the right of the black Mohr's circle) shows a perturbation in the shear stress of the elements immediately next to the salt.

Examples generated by the new application are shown in Figs. 11, 12, 13, and 14.

The application consists of multiple coordinated views, where the finite element model is displayed in one view and the Mohr diagram is displayed in another linked view, as shown in Fig. 4. We use brushing and linking as the interaction mechanism connecting the two views. The data set can be sliced (Fig. 11) or a variable can be thresholded (Fig. 9) to reduce the number of elements being viewed. The Mohr diagram window updates automatically to reflect changes in the model window.

In the model view, context is provided by wire frame or gray transparent renderings of the external faces of element groups that have significance within the model. Elements are color-coded based on the values of a user-selected

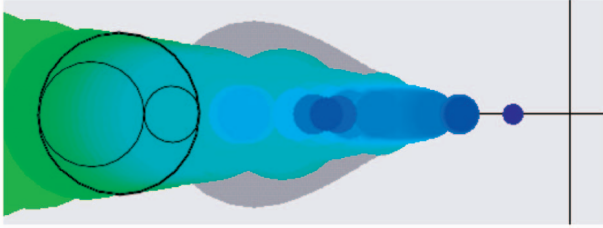


Fig. 5. Zoomed-in image of Mohr's circle detail in Fig. 4. The interactive Mohr's circle glyph is superimposed on both the colored subset envelope and the gray envelope showing the anisotropy for the entire model. All of the Mohr's circles are to the left of the origin, so they all indicate a compressive stress state. The rightmost blue circle results from the discrete nature of finite element meshes.

element variable. That variable's range of values is mapped onto a rainbow scale, where red represents high values and blue represents low values. The user can optionally display a legend in the model window correlating the values with the color range (Figs. 11, 13, and 14).

To provide context in the Mohr diagram window, the Mohr's circle for a particular element can be superimposed over color-coded layers, providing both global and subset information, as shown in Fig. 4 and the closeup in Fig. 5. This assists the analyst in developing a global understanding of the data, as well as locating those elements with the largest degree of anisotropy or isotropy or the greatest compressive or tensile forces.

For nonsymmetric tensors, we visualize the symmetric part using Mohr's circles and the nonsymmetric part (from either an additive or multiplicative decomposition) using a separate hedgehog field, rendered in the model window, showing the direction of the principle axis of the rotational vector associated with the nonsymmetric part, colored by its magnitude.

5.1 Contextual Information and Probing

We expand upon the traditional Mohr diagram by including global and subset information for model elements through a series of layers that can be drawn in the Mohr diagram window. These can be viewed separately or in combination.

First, the analyst can view global information drawn from the entire model. The combined footprints of the Mohr's circles for every element in the model produce a filled envelope that shows the global degree of anisotropy at each position along the horizontal axis. As shown in Fig. 4 and Fig. 5, this global envelope is drawn in gray as a background image in the Mohr diagram window.

Additionally, the analyst can overlay the global envelope with color-coded Mohr's circles for a subset of elements using the same color-coding as is used to render the subset of elements in the model window. An example of this overlay is shown in Fig. 4, where the colored Mohr's circles of the elements in the planar subset are drawn over the gray envelope for the entire model. Part of the underlying global envelope is still visible behind the cyan section, indicating that there are elements with greater anisotropy for approximately the same level of mean stress elsewhere in the model. The circles are drawn in order of size, from large to small so that the smaller, darker blue circles corresponding to the

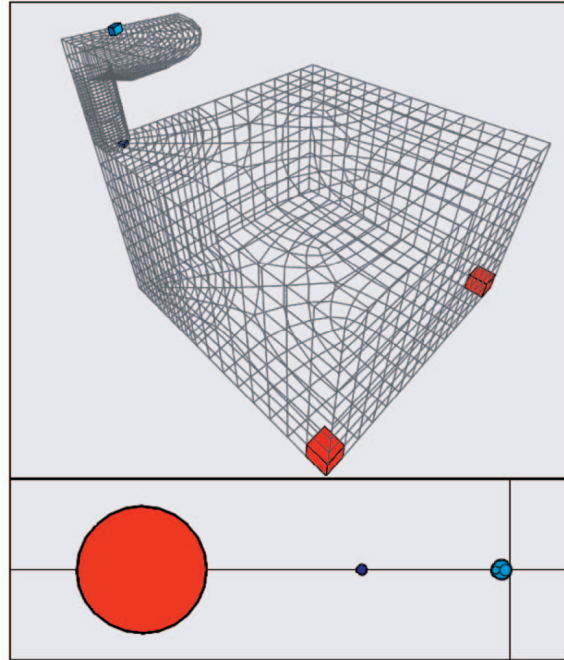


Fig. 6. The four Mohr's circle extrema and their associated elements within the model window are shown. Note that the red elements produce overlapping circles in the Mohr diagram window. Also, for clarity, several of the material blocks in the database are not shown in this visualization (namely, those surrounding the salt diapir). The rightmost Mohr's circle corresponds to an element in the layer immediately overlying the salt diapir and shows that the stress state of the sediment layer has three unequal eigenvalues. In contrast, the middle Mohr's circle corresponds to an element within the salt diapir and indicates an isotropic state of stress in the salt. The leftmost Mohr's circles correspond to elements far removed from the salt diapir and reveal a biaxial compressive stress state with two equal eigenvalues, i.e., the far-field stress state. This facilitates validation of the finite element analysis.

upper rows of the subset plane remain visible. Fig. 5 shows a zoomed-in view of this detail.

A third overlay is generated when we probe elements in the model window for stress information by using the Mohr's circle as a dynamic glyph that interactively changes as the mouse brushes over different elements in the model window. The glyph is a Mohr's circle consisting of a triad of black circles drawn over the color-coded subset envelope, as shown in the lower image in Fig. 4 and the closeup of the same image in Fig. 5.

Upon reading in a new data set, the application calculates the eigenvalues and eigenvectors for each tensor. The center point for each Mohr's circle is calculated as needed and the circles are sorted, first according to their size, then according to their position along the compression/tension (horizontal) axis. The circle extrema, circles with the largest and smallest sizes and the leftmost and rightmost coordinates along the horizontal axis, are found. These circles are the elements whose tensors represent the extremes in the anisotropic and/or isotropic distribution of forces and the extremes in compressive and/or tensile forces, respectively. An example of the four Mohr's circle extrema and their associated elements is given in Fig. 6. The Mohr's circles for the two red elements are so close to each other that they overlap. They can be seen as the largest, leftmost circle at the bottom of Fig. 6.

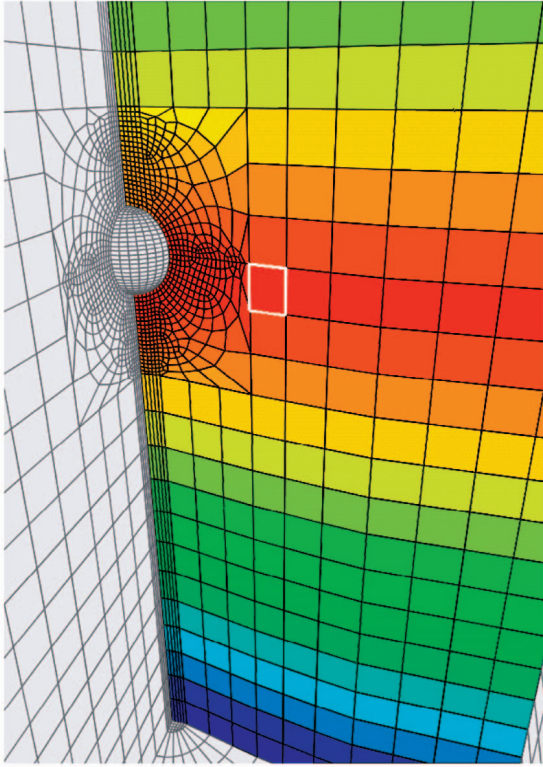


Fig. 7. Elements are color-coded by similarity to the selected element, which is highlighted in white. Red elements are most similar, while blue elements are least similar.

Clicking on an element within the model window selects it. A new variable can then be created to represent the distance between the eigenvalues of the selected element and the eigenvalues of the other elements in the model. We compute the distances by treating each element's eigenvalue triplet as a point in three-space, then calculating the Euclidean distance from each point to the selected cell's point. Recoloring the elements by this derived variable, as in Fig. 7, shows at a glance those elements that are most similar to the selected element (in red) and those that are most different (in blue).

5.2 Filtering

Selecting circles or specifying Mohr's circle parameters within the Mohr diagram window provides a filtering mechanism that links back to the model display window. For instance, all of the elements whose degree of compression is within some tolerance of a selected circle can be chosen or all the elements whose outer Mohr's circle radius (and degree of anisotropy) is equal to some value can be displayed. Alternatively, an element can be selected from within the model window and all elements whose Mohr's circle parameters are within some percentage of its parameters can be selected, as is shown in Fig. 8.

Filtering operations can be used to create new sets and to describe new element groups. These sets can be turned on and off interactively or combined with built-in sets from the simulation (things like elements grouped by material type or processor identifier). These new filtering operations are performed in combination with the filtering functions we

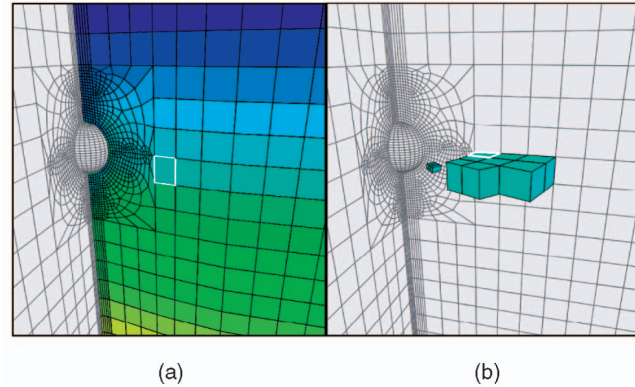


Fig. 8. (a) The selected element is outlined in white in the model window. (b) The model window has been updated to display the same element along with all of the elements whose Mohr's circles fall within 0.2 percent of its Mohr's circle parameters.

developed previously for scalar and vector variables. This provides a rich mechanism for querying the data set for elements that meet various criteria.

The filtering capability can be used, for example, to show only those elements in a calculation that are deforming elastically. Conversely, filtering can be used to display only elements that have yielded plastically or even to locate inadmissibly behaving elements, such as finite elements on the verge of inverting.

Filtering elements in the model based on Mohr's circle parameters vastly reduces clutter in a three-dimensional environment. Feature detection can be performed by filtering on either the isotropic extreme given by the Mohr's circle with the smallest radius or on circles that have two eigenvalues equal to one another [27]. This will locate the elements in the model containing degenerate points.

5.3 Rotation Information

For three-dimensional tensor values, principal orientations cannot be readily encoded into Mohr diagrams. Instead, we present this information in the model window. To visualize principal orientations in the application, the analyst can select from the two options, each of which was developed to support a different user community.

For the mechanics community, we provide a simple plot of the field of principal stress directions. Even though such a plot shows only two principal directions at a time, the orientation of the third eigenvector is implied by the relative orientations of the two directions that are seen. We draw the eigenvectors as a cross to reduce the visual clutter and make the image more intelligible. The user can understand the orientation by interactively changing the view.

The second option for visualizing principal directions in three dimensions considers the matrix of direction cosines to be a rotation matrix and applies the Euler-Rodrigues theorem [15] to plot the axis of rotation colored by the angle of rotation. This option has considerable appeal to the geomechanics community because the direction cosine matrix can be made unique by using eigenvectors that are orthonormalized projections of the laboratory base vectors onto the eigenspaces (allowing visualization of the unique

smallest rotation angle needed to transform the laboratory basis into the principal basis).

6 APPLICATION AND RESULTS

The goal of our numerical analyses is to identify drilling trajectories that minimize risk, while also providing ready access to the desired exploration target or, in the case of a sanctioned development, compatibility with the field development plan.

GoM near-salt and subsalt reservoir settings include a variety of geometric configurations, including spherical diapirs, columnar diapirs, columnar diapirs with tongues, and thick, flat-lying sheets [13]. We limit our discussion here to static spherical (Fig. 4) and columnar diapir models (Fig. 6). The spherical model contains 8,136 elements, while the columnar model contains 10,128 elements. Additionally, we describe application to a model containing over a million elements developed for a specific field setting.

For each data set, we are interested in examining tensor information for elements in and near the salt formation and contrasting their behavior with elements in regions that are removed from the influence of the salt diapir, known as the *far-field*. Stresses in the far-field reflect a passive sedimentary basin setting in which gravitational loading results in a stress state where the vertical stress, S_V , is due to the weight of the overburden and the horizontal stress, S_H , is equal to some fraction of S_V [30]. However, this stress state cannot be sustained within salt formations, where the stresses relax to reach an isotropic state with $S_H = S_V$. This stress state is at odds with the surrounding sands and shales, which can support a deviatoric state of stress with $S_H \neq S_V$. Because the salt diapir is in equilibrium and maintains continuity with the surrounding formations, the stress state near the interface is complex and perturbed from the far-field state. The only way to determine the local stresses is to solve the complete set of equilibrium, compatibility, and constitutive equations with the appropriate initial and boundary conditions; in the current work, this is accomplished via numerical finite-element simulation.

Several aspects of the near-salt stress field are significant in the context of reducing drilling risks. First, we seek to identify locations where shear stresses are locally elevated because this impacts wellbore stability. Second, it is important to identify regions where horizontal stresses are locally reduced because this likewise affects wellbore stability by impacting *fracture gradient*, which is the stress at which the formations surrounding the wellbore will fracture. Third, regions where the vertical stresses are perturbed from the far-field must be identified to support calculations of the drilling pressures required for wellbore stability. Finally, identification of optimal drilling paths is also impacted by regions where the principal stress directions (eigenvectors) have rotated relative to the vertical and horizontal directions that characterize the far-field.

We illustrate the fourth interest above first because, as discussed in the previous section, visualization of stress rotations is typically difficult for the geomechanics and mechanics user communities. Stress rotation is illustrated with the spherical geometry in Fig. 9, where we show a group of elements where the principal stresses have rotated from

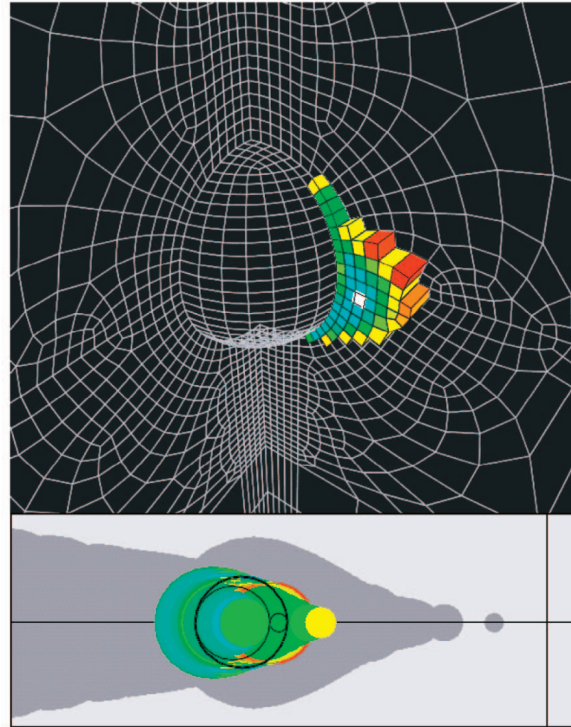


Fig. 9. Filtering on the amount of rotation, we have isolated this planar slice through a clump of elements in the vicinity of a spherical salt diapir. The Mohr's circles for the subset are then overlaid on the envelope from the entire model. The Mohr's circle for the element shown in white is displayed in black and reveals a triaxial compressive stress state with three unequal eigenvalues indicating the near-salt stress perturbation. (As discussed in Fig. 6, the stress state in the far-field is characterized by two equal eigenvalues.)

vertical and horizontal, which affects wellbore stability while drilling [13]. Filtering the model window to display just a single plane of elements, we superimpose their Mohr's circles on the envelope (shown in gray) for the entire model. As we interactively probe the cells, the black Mohr's circle overlays the colored circles for the subset. The current element is drawn in white in the model view and its particular Mohr's circle overlays the colored circles for the subset.

This latter aspect is illustrated for the columnar diapir with tongue model database in Fig. 10. In this example, we have filtered on those elements that display a high degree of rotation and then colored-coded a subset of these elements, based on the degree of rotation and scaled by their magnitude within the selected range.

For the same database, we visualize the local reductions in the maximum principal stress that can occur adjacent to salt diapirs (note that, because compressive stresses are defined as negative, this is the eigenvalue that is smallest in magnitude). Fig. 11 shows the changing values of the maximum principal stress, which is proportional to the fracture gradient. One can readily evaluate the length scale of the stress perturbations and locate "hot spots" with respect to the location of the columnar salt diapir and overlying salt tongue.

In Fig. 12, we illustrate another useful application of the filtering capability where we identify elements outside of the spherical salt diapir in which the von Mises stress is elevated above a threshold value of 45 MPa. Because it is an

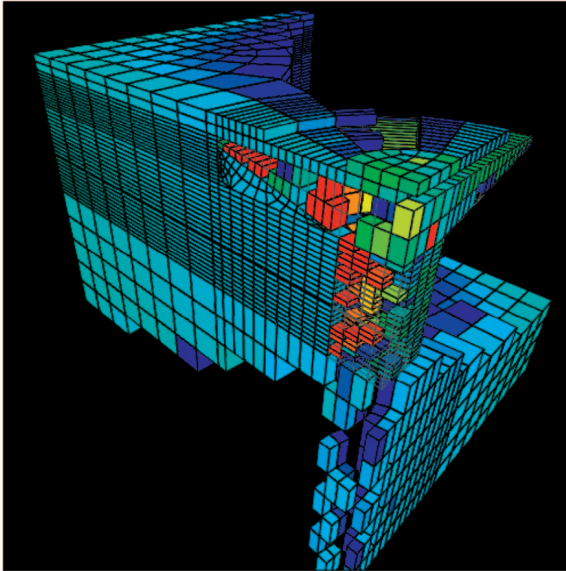


Fig. 10. Salt pillar model elements filtered for highest stress rotation.

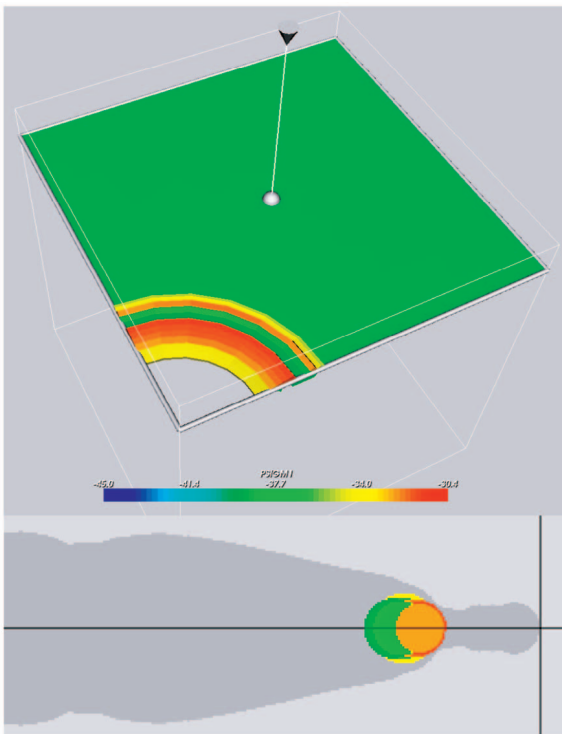


Fig. 11. Planar horizontal cut through the columnar diapir model showing the value of the eigenvector λ_1 equal to the minimum principal stress (recall that compression is defined as negative). The widget for manipulating the cutting plane is visible in the center of the model view. Because the cutting plane is at a shallow depth in the model, the colored Mohr's circles are all indicative of low mean stresses. The minimum principal stress is elevated above the far-field values immediately below the salt tongue, as can be seen by the *hotter* colors. The overlay of the colored Mohr's circles against the gray envelope from the rest of the model provides a background context for how shear stress on this plane compares to the rest of the model.

invariant, the von Mises stress, equal to the square root of one-half of the sums of the squares of the principle stress differences, is a convenient measure of the shear (deviatoric) stress, which, as noted above, affects wellbore

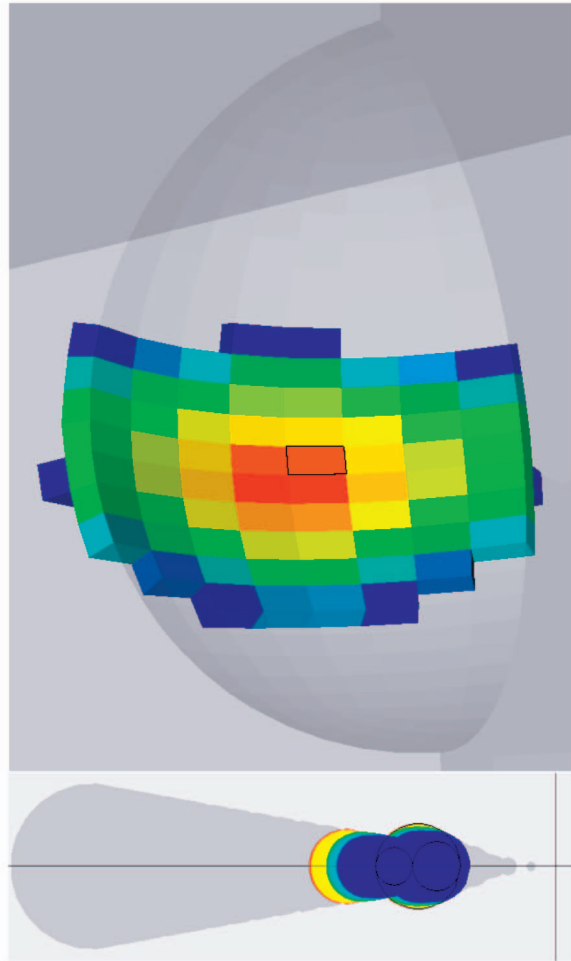


Fig. 12. Filtering on the von Mises stress value, we have isolated this shell of elements at the interface with the spherical salt diapir. In the Mohr diagram, the Mohr's circle for the selected element (highlighted in black) overlays a colored envelope for the selected elements, which, in turn, overlays the gray envelope for the entire model. For the element shown, the intermediate eigenvalue, λ_2 , is almost midway between the minimum and maximum eigenvalues, indicating a stress state highly perturbed from the far-field (where two eigenvalues are equal).

stability. For the application of interest, this visualization is particularly useful because the analyst can immediately see whether the von Mises stress is elevated due to a difference between only two principal stress values or whether it is elevated because all three three principal stresses are unequal—the two scenarios have potentially different implications for wellbore stability. In the particular example shown, the visualization also illustrates small inaccuracies in the numerical analysis that result from the mesh resolution and the approximation of a spherical shape using hexahedral elements. Depending upon the requirements of the analysis, this may encourage the analyst to remesh this region to gain higher accuracy.

The final example we consider is a large, multimillion-element model that was constructed to represent a real field setting. In Fig. 13 and Fig. 14, in which the large salt diapir is not shown, we present two different visualizations of the von Mises stress in the formations immediately next to the salt diapir and tongue that abut hydrocarbon-rich formations. The visualization in Fig. 13 shows shear stress in the

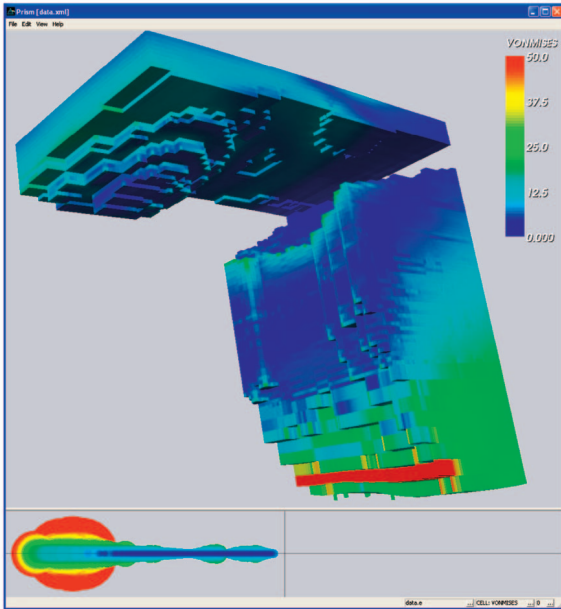


Fig. 13. Visualization of the invariant shear stress in the material block lying immediately to the right, and above, an irregularly shaped salt diapir (note that the salt material block is not shown). The Mohr's circles shown in red indicate the elevated shear stresses adjacent to the salt diapir.

material face immediately next to the salt diapir, whereas the visualization in Fig. 14 shows shear stress along a vertically oriented plane that transects the formation next to the salt diapir. Such information can suggest salt exit points that minimize shear stress on the wellbore.

7 CONCLUSIONS

The tensor visualization methods developed in this work are directly motivated by the data analysis needs of the mechanics community. Deterministic finite-element analysis tools and, particularly, those used in defense-related applications, have reached a highly developed state of maturity. The code used here, JAS3D [2], utilizes explicit quasistatic solvers developed specifically under US Department of Energy (DOE) Defense Programs to handle very large deformation problems with complex material constitutive models and contact surfaces. The code is based on massively parallel, distributed memory multiprocessor computers, enabling analysis of models containing tens of millions of finite elements. JAS3D is ideally suited for geomechanics problems because it supports highly non-linear material behavior, large-deformations, and a high degree of geometric complexity [14]. With the significant advancement in computational capabilities experienced over the past decade and advances in constitutive modeling of geomaterials [11], it is now practical to perform analyses of complex field settings that may require tens of millions of finite elements to accurately represent the complex geologic structure and achieve adequate resolution in specific regions of interest.

The ability to perform such sophisticated numerical analyses does not come without cost. First, as model complexity increases, it becomes increasingly difficult for

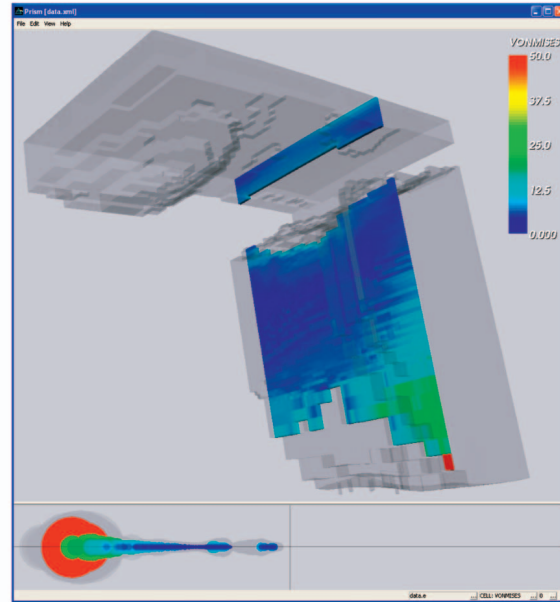


Fig. 14. This is an alternative visualization of the data shown in Fig. 13. This shows the von Mises stress in a vertically oriented plane of elements that are lying in the formation next to the salt diapir. The salt material block that represents the diapir is not shown. The gray envelope represents the element stress values excluded from the planar cut that is shown. Cutting through the complicated geometry allows closer inspection of the stress perturbations as we interactively slide the cutting plane back and forth.

the analyst to verify the integrity of the numerical analysis and that it is free from artifacts introduced, for example, by inadequate mesh resolution or by approximations of the far-field boundary conditions. Second, after model assurance is achieved, the analyst is still faced with interpreting a vast array of second-order tensor data that exhibits considerable complexity in space and, for some analyses, in time. The increased sophistication of numerical analysis codes and high-performance computing capabilities have generally outstripped the suite of postprocessing tools available to the analyst for interpretation. The work described here addresses both needs by providing a suite of visualization tools on par with the sophisticated numerical analyses codes and supercomputers that are currently available.

Because physicists and engineers have used Mohr's circles for the last 100 years, an interactive visualization tool based on Mohr diagrams is immediately useful with virtually no learning curve for the material mechanics and geomechanics analyst. This paper demonstrates the usefulness of Mohr diagrams to the visualization community by illustrating their use in a geomechanics application. The interactive Mohr circle glyph, when viewed in concert with other stress data (for example, von Mises stress), provides an environment for data analysis that is both vastly simplified and highly intuitive. It communicates a large amount of information in a relatively small area of the screen.

Further development of Mohr diagram visualization is already underway for other advanced applications aimed at debugging finite element codes (for example, by locating nearly inverted elements or identifying regions in which solutions may be affected by mesh resolution or element aspect ratio) and visualizing differences between solution

methods in these codes. For the latter goal, we are currently addressing the comparison of solutions generated by Eulerian versus Lagrangian implementations in order to quantify the errors introduced by each of these approaches.

ACKNOWLEDGMENTS

The authors thank Brian Wylie and also acknowledge Billy Joe Thorne, Arlo Fossum, and Rick Garcia for their contributions to the larger geomechanical modeling effort. The US Department of Energy (DOE) Mathematics, Information, and Computer Science Office funded the visualization portion of this work. The geomechanics research was performed under an ongoing Joint Industry Project cofunded by the DOE Office of Fossil Energy Natural Gas and Oil Technology Partnership Program and an industry consortium including BP, ChevronTexaco, BHP Billiton, ConocoPhillips, ExxonMobil, Kerr-McGee, Petrobras S.A., and Shell. This work was performed at Sandia National Laboratories, a multiprogram laboratory operated by Sandia Corporation, a Lockheed Martin Company, for the US Department of Energy's National Nuclear Security Administration under Contract DE-AC04-94AL85000.

REFERENCES

- [1] J. Blanchette and M. Summerfield, *C++ GUI Programming with Qt 3*. Upper Saddle River, N.J.: Prentice Hall in association with Trolltech Press, 2004.
- [2] M.L. Blandford, "JAS3D—A Multi-Strategy Iterative Code for Solid Mechanics Analysis," Users' Instructions, Release 1.6, Sandia Nat'l Laboratories Internal Memorandum, Sept. 1998.
- [3] E. Boring and A. Pang, "Interactive Deformations from Tensor Fields," *Proc. IEEE Visualization '98*, pp. 297-304, 1998.
- [4] W.B. Bradley, "Borehole Failures Near Salt Domes," *Proc. 1978 Ann. Fall Technical Conf. and Exhibition*, paper SPE 7503, Oct. 1978.
- [5] R. Brannon, "Mohr's Circle and More Circles," http://www.me.unm.edu/~rmbbrann/Mohrs_Circle.pdf, 2003.
- [6] P. Crossno and D.H. Rogers, "Visual Debugging," *IEEE Computer Graphics and Applications*, vol. 22, no. 6, pp. 6-10, Nov./Dec. 2002.
- [7] P. Crossno, D.H. Rogers, R.M. Brannon, and D. Coblentz, "Visualization of Salt-Induced Stress Perturbations," *Proc. IEEE Visualization 2004*, pp. 369-376, 2004.
- [8] P. Crossno, D.H. Rogers, and C.J. Garasi, "Case Study: Visual Debugging of Finite Element Codes," *Proc. IEEE Visualization 2002*, pp. 517-520, 2002.
- [9] W.C. de Leeuw and J.J. van Wijk, "A Probe for Local Flow Field Visualization," *Proc. IEEE Visualization '93*, pp. 39-45, 1993.
- [10] T. Delmarcelle and L. Hesselink, "Visualization of Second Order Tensor Fields and Matrix Data," *Proc. IEEE Visualization '92*, pp. 316-323, 1992.
- [11] A.F. Fossum and R.M. Brannon, "The Sandia GEOMODEL: Theory and User's Guide," Technical Report SAND2004-3226, Sandia Nat'l Laboratories, Albuquerque, N.M., 2004.
- [12] A.F. Fossum and J.T. Fredrich, "Salt Mechanics Primer for Near-Salt and Sub-Salt Deepwater Gulf of Mexico Field Developments," Technical Report SAND2002-2063, Sandia Nat'l Laboratories, Albuquerque, N.M., 2002.
- [13] J.T. Fredrich, D. Coblentz, A.F. Fossum, and B.J. Thorne, "Stress Perturbations Adjacent to Salt Bodies in the Deepwater Gulf of Mexico," *Proc. 78th Ann. Technical Conf. and Exhibition*, SPE 84554, pp. 1-14, 2003.
- [14] J.T. Fredrich and A.F. Fossum, "Large-Scale Three-Dimensional Geomechanical Modeling of Reservoirs: Examples from California and the Deepwater Gulf of Mexico," *Oil and Gas Science and Technology—Revue de L'IFP*, vol. 57, no. 5, pp. 423-441, 2002.
- [15] H. Goldstein, C.P. Poole Jr., and J.L. Safko, *Classical Mechanics*. Columbia Univ.: Addison-Wesley, 2002.
- [16] R. Haber, "Visualization Techniques for Engineering Mechanics," *Computing Systems in Eng.*, vol. 1, no. 1, pp. 37-50, 1990.
- [17] Y.M.A. Hashash, D.C. Wotring, J.I.-C. Yao, J.-S. Lee, and Q. Fu, "Visual Framework for Development and Use of Constitutive Models," *Int'l J. Numerical and Analytical Methods in Geomechanics*, vol. 26, pp. 1493-1513, 2002.
- [18] L. Hesselink and J.J. van Wijk, "Research Issues in Vector and Tensor Field Visualization," *IEEE Computer Graphics and Applications*, vol. 14, no. 2, pp. 76-79, Mar. 1994.
- [19] L. Hesselink and J.J. van Wijk, "The Topology of Symmetric, Second-Order 3-D Tensor Fields," *IEEE Trans. Visualization and Computer Graphics*, vol. 3, no. 1, pp. 1-11, Jan.-Mar. 1997.
- [20] B. Jeremić, G. Scheuermann, J. Frey, Z. Yang, B. Hamann, K.I. Joy, and H. Hagen, "Tensor Visualizations in Computational Geomechanics," *Int'l J. Numerical and Analytical Methods in Geomechanics*, vol. 26, pp. 925-944, 2002.
- [21] G. Kindlmann, "Superquadric Tensor Glyphs," *Proc. VisSym 2004*, pp. 147-154, 2004.
- [22] G. Kindlmann and D. Weinstein, "Hue-Balls and Lit-Tensors for Direct Volume Rendering of Diffusion Tensor Fields," *Proc. IEEE Visualization '99*, pp. 183-189, 1999.
- [23] G. Kindlmann, D. Weinstein, and D. Hart, "Strategies for Direct Volume Rendering of Diffusion Tensor Fields," *IEEE Trans. Visualization and Computer Graphics*, vol. 6, no. 2, pp. 124-138, Apr.-June 2000.
- [24] R.M. Kirby, H. Marmanis, and D.H. Laidlaw, "Visualizing Multivalued Data from 2D Incompressible Flows Using Concepts from Painting," *Proc. IEEE Visualization '99*, pp. 333-340, 1999.
- [25] R.D. Kriz, E.H. Glaessgen, and J.D. MacRae, "Eigenvalue-Eigenvector Glyphs: Visualizing Zeroth, Second, Fourth and Higher Order Tensors in a Continuum," *Proc. NCSA Workshop Modeling the Development of Residual Stresses during Thermoset Composite Curing*, Sept. 1995.
- [26] D. Laidlaw, E.T. Ahrens, D. Kremers, M.J. Avalos, R.E. Jacobs, and C. Readhead, "Visualizing Diffusion Tensor Images of the Mouse Spinal Cord," *Proc. IEEE Visualization '98*, pp. 127-134, 1998.
- [27] Y. Lavin, Y. Levy, and L. Hesselink, "Singularities in Nonuniform Tensor Fields," *Proc. IEEE Visualization '97*, pp. 59-66, 1997.
- [28] M.A. Livingston, "Visualization of Rotation Fields," *Proc. IEEE Visualization '97*, pp. 491-494, 1997.
- [29] K. Martin and B. Hoffman, *Mastering CMake*. Kitware, Inc., 2003.
- [30] A. McGarr and N.C. Gay, "State of Stress in the Earth's Crust," *Ann. Rev. Earth Planet. Science*, vol. 6, pp. 405-436, 1978.
- [31] F.J. Post, T. van Walsum, F.H. Post, and D. Silver, "Iconic Techniques for Feature Visualization," *Proc. IEEE Visualization '95*, pp. 288-295, 1995.
- [32] W. Schroeder, K. Martin, and W. Lorensen, *The Visualization Toolkit: An Object-Oriented Approach to 3D Graphics*, third ed. Kitware, Inc., 2002.
- [33] K. Seymour, G. Rae, J. Peden, and K. Ormston, "Drilling Close to Salt Diapirs in the North Sea," *Proc. Offshore European Conf.*, paper SPE 26693, Sept. 1993.
- [34] A. Sigfridsson, T. Ebbens, E. Heiberg, and L. Wigström, "Tensor Field Visualisation Using Adaptive Filtering of Noise Fields Combined with Glyph Rendering," *Proc. IEEE Visualization '02*, pp. 371-378, 2002.
- [35] R. Sweatman, R. Faul, and C. Ballew, "New Solutions for Subsalt-Well Lost Circulation and Optimized Primary Cementing," *Proc. 1999 SPE Ann. Technical Conf. and Exhibition*, paper SPE 56499, Oct. 1999.
- [36] D. Weinstein, G. Kindlmann, and E. Lundberg, "Tensorlines: Advection-Diffusion Based Propagation through Diffusion Tensor Fields," *Proc. IEEE Visualization '99*, pp. 249-253, 1999.
- [37] B.-F. Westin, S.E. Maier, H. Mamata, A. Nabavi, F.A. Jolesz, and R. Kikinis, "Processing and Visualization for Diffusion Tensor MRI," *Medical Image Analysis*, vol. 6, pp. 93-108, 2002.
- [38] B. Wünsche and A. Young, "The Visualization and Measurement of Left Ventricular Deformation Using Finite Element Models," *J. Visual Languages & Computing*, vol. 14, no. 4, pp. 299-326, 2003.
- [39] X. Zheng and A. Pang, "Volume Deformation for Tensor Visualization," *Proc. IEEE Visualization 2002*, pp. 379-386, 2002.
- [40] X. Zheng and A. Pang, "Interaction of Light and Tensor Fields," *Proc. VisSym 2003*, pp. 157-166, 295, 2003.



Patricia Crossno received the PhD degree in computer science from the University of New Mexico in 1998. After finishing her doctorate, she joined the Data Analysis and Visualization department at Sandia National Laboratories. She has served as the principal investigator on several research grants from the US Department of Energy's Office of Mathematics, Information, and Computer Science, including a current project in hardware-accelerated visualization.

She has authored papers on a variety of visualization topics. Her current research interests are scientific and information visualization, visual data mining, and multiple, coordinated-view user interfaces. She is active in reviewing research proposals and technical papers and she has served on a number of conference program committees, including IEEE Visualization. She is a member of the IEEE and the ACM.



David H. Rogers received the BA degree in architecture with honors from Princeton University in 1988 and the MS degree in computer science from the University of New Mexico in 1996. He cofounded and served as president of the startup company, dynaVu, Inc., which developed a patented graphical user interface for viewing large data sets. He went on to work at Dreamworks SKG Feature Animation, where his credits included production software supervisor for *Spirit: Stallion of the Cimarron*. He is currently working in the

Data Analysis and Visualization Department at Sandia National Laboratories.



Rebecca M. Brannon received the PhD degree in 1993 from the University of Wisconsin. She specializes in computational tensor analysis applied to inelasticity of geological materials, ceramics, ferroelectrics, and metals. She has been employed since 1993 at Sandia National Laboratories (and has had appointments with Los Alamos National Laboratory, the US Air Force Research Laboratory, and the University of New Mexico). By invitation from TU Delft's

research school, she recently conducted an international short course based on her Internet book, *Functional and Structured Tensor Analysis for Materials Modeling*. She is an adjunct professor and university accreditor for the American Society of Mechanical Engineers. Having served as an organizer for the American Physical Society (APS) Shock Compression of Condensed Matter Conference, she contributed an invited book chapter on plasticity for an upcoming APS-sponsored shock physics handbook. She gave a keynote presentation at the Plasticity 2005 conference.



David Coblenz received the BA degree in physics/earth science with a German literature minor in 1985 from the University of California at San Diego, the MS degree in geophysics in 1988 from Boston College, and the PhD degree in geophysics in 1994 from the University of Arizona. He is a solid earth geophysicist with a joint appointment at the Los Alamos National Laboratory and the University of New Mexico who, through speculative geodynamics research, seeks the common ground between plate tectonics and geocology. His research interests include solid-earth geophysics, geodynamics, geocology, and biogeography.



Joanne T. Fredrich received the PhD degree in geophysics from the Massachusetts Institute of Technology and the BS (honors) degree in geology from the State University of New York at Stony Brook. She is a distinguished member of the technical staff in the Geophysics Department at Sandia National Laboratories in Albuquerque, New Mexico. Her interests include geomechanics, rock physics, and three-dimensional imaging and fluid flow in porous media.

She is a current member of the National Research Council's Committee on Geological and Geotechnical Engineering and of the Editorial Review Committee of the Society of Petroleum Engineering and she is a past associate editor for the *Journal of Geophysical Research*.

► **For more information on this or any other computing topic, please visit our Digital Library at www.computer.org/publications/dlib.**